Bingham Research Center
UtahStateUniversity

FINAL REPORT

AIR POLLUTANT EMISSIONS FROM NATURAL GAS-FUELED PUMPJACK ENGINES IN THE UINTA BASIN

Seth Lyman
Huy Tran
Trevor O'Neil
Marc Mansfield

DOCUMENT NUMBER: BRC_211231B
REVISION: REVISION 1
DATE: 11 MARCH 2022

(435) 722-1740 320 North Aggie Boulevard Vernal, Utah 84078 binghamresearch.usu.edu

Executive Summary

We measured a comprehensive suite of pollutants emitted from 58 natural gas-fueled pumpjack engines in Utah's Uinta Basin between January and May 2021, with repeat measurements of five engines in January 2022. We documented the emissions composition of several makes and models of commonly used engines, including Ajax E42, E565, DP60, and DP80 engines; Arrow L795, C101, and C106 engines; and GM Vortec.

Air-fuel ratios (i.e., the ratio of air taken in by the engine to the amount of air needed for combustion of the fuel) were strong predictors of emissions. Higher air-fuel ratios (i.e., engines that take in more air than needed for combustion) led to lower oxides of nitrogen (NO_X) emissions and higher emissions of organic compounds. Engines with air-fuel ratios greater than three tended to have very low NO_X emissions and a large percentage of the fuel gas passing through the engine uncombusted. Low air-fuel ratios were associated with more complete combustion, higher NO_X, and the formation of more reactive organic compounds, including alkenes and carbonyls.

Average NO_X emissions in this study were only 9% of average emissions from natural gas-fueled pumpjack engines in version 1.89 of the Utah Division of Air Quality oil and gas emissions inventory. In contrast, volatile organic compound emissions in the study were 15 times higher than in the inventory. When we applied averages from our measurements to inventoried pumpjack engines, we found that emissions from all types of engines dropped from 58% to 37% of total inventoried NO_X and increased from 2% to 16% of total inventoried volatile organic compounds. Emissions of formaldehyde and carbon monoxide from engines were also higher than inventoried values.

Contents

List of Tables

List of Figures

1. Background and Significance

Areas of the Uinta Basin below an elevation of 6,250 feet are classified by the U.S. Environmental Protection Agency (EPA) as a marginal nonattainment area for ozone. Its designation may be changed to moderate, which will trigger a requirement for the regulatory agencies to develop an Implementation Plan that brings the Basin into attainment of the EPA ozone standard. As part of this plan, agencies will be required to develop regulations to reduce emissions and show with three-dimensional photochemical modeling that those regulations will reduce ozone enough to achieve attainment of the standard.

Our team's current meteorological model for winter 2013 reproduces meteorological quantities with reasonable accuracy (Tran and Tran, 2021). When we use this meteorological model with version 1.89 of the Utah Division of Air Quality emissions inventory (UDAQ, 2021) in the CAMx photochemical transport model, simulated ozone concentrations are too low. There may be several reasons for this under-representation of ozone in photochemical models, but one reason appears to be that inventoried emissions of reactive organics from oil and gas sources are lower than reality (Lyman et al., 2021a; Tran et al., 2021). In particular, carbonyls and alkenes are too low in photochemical simulations. These compound groups are very important for wintertime ozone production (Edwards et al., 2014; Lyman et al., 2021a).

Many potential sources of reactive organics in the Uinta Basin are inadequately characterized, and recent work completed by the Utah Division of Air Quality and others has helped to fill in some of these gaps (Lyman and Tran, 2015; Lyman et al., 2021a; Lyman and Mansfield, 2018; Lyman et al., 2018; Lyman et al., 2017; Mansfield et al., 2018; Tran et al., 2021; Tran et al., 2017; Wilson et al., 2020). Little has been done to improve understanding of emissions from combustion sources, however (Lyman et al., 2021a). For example, the only estimate of the composition of organic compound emissions from pumpjack (a.k.a., artificial lift) engines available in the EPA SPECIATE database (EPA, 2020) for use in photochemical models is based on measurements of just a handful of engines conducted in California in 1985 (Oliver and Peoples, 1985). Also, estimates of the magnitude of emissions of oxides of nitrogen (NO_X) and organics in official inventories are largely derived either from AP-42 emission factors (EPA, 1995) or manufacturer's specifications, rather than from field measurements. Engine emissions are a significant portion of official inventories (59% of total NO_X and 2% of total organics from oil and gas; UDAQ (2021)). Measurements of engine emissions in real field conditions in the Uinta Basin are needed to improve the ability of photochemical models to simulate wintertime ozone.

2. Objectives

The objective of this study at its outset was to measure as-found emissions of oxides of nitrogen (NO and NO_2), carbon dioxide, oxygen, carbon monoxide, methane, a suite of 52 non-methane hydrocarbons, three light alcohols, and thirteen carbonyls from about 50 natural gas-fueled pumpjack engines in the Uinta Basin. We also planned to modify engine operating conditions for an additional 5-10 engines to determine how engine operating parameters impact emissions magnitude and composition. See Section 4 for a description of deviations from these original objectives.

3. Methods

3.1. Statistical Methods

We calculated bootstrapped 95% confidence limits around means using the scikits.bootstrap tool in Python. We report values in this document as mean (lower confidence limit, upper confidence limit).

3.2. Definition of VOC

In the regulatory world, the word Volatile Organic Compounds (VOC) is typically used to mean organic compounds that are more reactive than ethane (see https://www.epa.gov/air-emissions-inventories/what-definition-voc). Usually, this means it includes all organic compounds except methane and ethane. For this study, we measured methane, ethane, and many other organic compounds explicitly. We include ethane and methane throughout the text of this document, except for in Section 5.8, where we compare our organic compound results to values from an emissions inventory. Official emissions inventories follow the regulatory definition of VOC, so we removed methane and ethane from our total organic compound emission results before comparing those results to inventoried values.

3.3. Engines Measured

We measured emissions from 58 engines belonging to 3 companies (referred to in this text and the final dataset as Companies A, B, and C) in Uintah and Duchesne Counties, Utah, between January and May 2021. We re-sampled 5 of these engines in January 2022. Table 3-1 provides a summary of the engines measured.

Table 3-1. Engines measured for this study. Inventory refers to version 1.89 of the Utah Division of Air Quality oil and gas emissions inventory.

	Horsepower	Type	Count in study	Percent of total in study	Percent of total in inventory
Ajax E42	40	one cylinder, two-stroke	22	37.9%	25.8%
Ajax E565	40	one cylinder, two-stroke	7	12.1%	11.6%
Ajax DP60	58	one cylinder, two-stroke	6	10.3%	2.2%
Ajax DP80	77	one cylinder, two-stroke	1	1.7%	0.3%
Arrow C101	24.5	one cylinder, two-stroke	9	15.5%	11.9%
Arrow C106	32	one cylinder, two-stroke	4	6.9%	5.2%
Arrow L795	65	two cylinders, two-stroke	7	12.1%	31.9%
GM Vortec 4.3L	195	six cylinders, four-stroke	2	3.4%	0.2%

3.4. Field Measurements

3.4.1. Meteorology

During each engine measurement, we measured ambient temperature and relative humidity (New Mountain NM150WX), wind speed and direction (Gill WindSonic), and barometric pressure (Campbell CS100) on a tower extended from the measurement trailer to a height of 6 m. We checked these measurements against NIST-traceable standards annually.

3.4.2. Detection of Non-exhaust Emissions

We planned to use our high-flow measurement system (Wilson et al., 2020) to quantify emissions from non-exhaust sources we found. To this end, we used a Bascom Turner Gas Rover (a handheld natural gas detector) to detect combustible gas emissions from oil vents and other possible non-exhaust sources on the first half of the engines we encountered. The Gas Rover has a detection limit of 10 ppm. Most engines had oil reservoir vents, and the air immediately around the vents occasionally had detectable combustible gas concentrations, sometimes reaching as high as several hundred ppm. We never detected emissions from any other non-exhaust source. We did not measure emissions from any of the emitting oil reservoir vents because:

1. The high flow system creates a vacuum to pull in emitted gas. Since the oil reservoir is at atmospheric pressure, subjecting it to a vacuum would create an artificially high emission rate.

2. Oil reservoir vents were located behind the engine's flywheel, making it impossible for us to access them safely.

3.4.3. Collection of Fuel Gas Samples

We collected fuel gas samples from 17 engine measurement locations in inert-coated stainless steel 500 mL sampling canisters with stainless steel valves on both ends. We connected the canisters to existing sampling ports on fuel gas lines at well pads (i.e., lines that connected to engines to supply gas used by the engines as fuel), opened both canister valves, and allowed fuel gas to flow through the canisters for about 60 seconds. We then closed the downstream canister valve, followed by the upstream valve, to collect each sample. We analyzed the samples in the laboratory for C1-C10 hydrocarbons and C1-C3 alcohols as described in Section 3.5.1.

3.4.4. Engine Properties

The pumpjack engines we encountered did not have reliable gauges to indicate rotations per minute (RPMs), engine temperature, or other engine properties. We estimated RPMs by tapping out the number of audible rotations over a period (usually 30 seconds) on a smartphone app and dividing the number of rotations by the time. This method is likely unreliable, but it may have some connection to reality. Our RPM measurements were within the range of manufacturer specifications. The GM Vortec engines operated at >1000 RPMs, making the aural measurement method impossible. We obtained RPM data for these engines from the site operator.

3.4.5. Physical Properties of Exhaust Stacks

We wrote a physical description of each engine's exhaust apparatus and estimated the height of each exhaust stack to within 0.3 m. We used a digital caliper to measure the internal diameter of each exhaust stack at its exit.

3.4.6. Physical and Inorganic Chemical Measurements of Engine Exhaust

We used an Ecom J2KN Pro Industrial analyzer to measure the physical and inorganic chemical properties of exhaust. The analyzer utilized standard sensors for oxygen (O_2), water vapor, carbon monoxide (CO), nitrogen monoxide (NO), and nitrogen dioxide (NO_2) and an infrared sensor for carbon dioxide (CO_2). We inserted the instrument's standard 0.3 m sampling probe with pistol grip into exhaust stacks a few minutes before recording measurements and began recording after measurements stabilized. We attached a 13 mm diameter stainless steel tube to the instrument's sampling probe when it was possible to insert the probe deeper than 0.3 m into the stack (see Section 3.7.6 for more information about the importance of probe depth). We collected measurements every 2 sec over 10 min periods in most cases.

The Ecom analyzer's probe incorporated a thermocouple to measure exhaust temperature, and the analyzer also measured exhaust pressure.

The Ecom analyzer was calibrated by the manufacturer before and at the end of the study. We also calibrated chemical measurements weekly during the study. Calibration results are available in Section 3.7.

3.4.7. Sampling Line for Organic Compounds

We sampled organic compounds via a custom-built heated sampling line. The tip was a 1.3 cm stainless steel tube. We used tubes of different lengths, depending on the stack depth (see Section 3.7.6). The maximum length used was 1.5 m. We inserted the probe into the end of the exhaust stack to collect exhaust gas samples. Downstream of the stainless tube was a stainless steel sintered filter (7 µm pore size) and a PFA Teflon filter pack that held a 47 mm PTFE filter with 5 µm pore size. After the filter pack was a 1 cm PFA Teflon tube of 15 m length. The final 0.5 m of the stainless tube, the filters, and all the Teflon tubing were heated to 55°C, which was hotter than the dewpoint of the exhaust samples. The sample line led to a generator-powered trailer, and sample gas was flushed through the line at 4 L min^{-1}.

3.4.8. Methane

We used a Los Gatos Research Fast Greenhouse Gas Analyzer with a high-concentration laser to measure methane concentrations in the exhaust gas. The analyzer pulled gas from the sample line in the trailer.

3.4.9. Non-methane Hydrocarbons and Alcohols

Within the trailer, evacuated silonite-coated 6 L stainless steel canisters with flow regulated by Alicat mass flow controllers collected gas samples from the sample line. The line to the canisters, and the canisters themselves, were unheated (the trailer itself was heated, but its temperature fluctuated with the ambient temperature and with opening and closing of doors). We analyzed filled canisters in our laboratory (see Section 3.5.1).

3.4.10. Carbonyls

An independent pump pulled exhaust gas from the sample line through Waters SepPak 2,4 dinitrophenylhydrazine (DNPH)-coated amorphous silica bead cartridges (350mg), which collected carbonyl compounds. We used two cartridges in series, which allowed the second cartridge to capture any breakthrough. The line to the cartridges and the cartridges themselves were heated to 55°C to avoid water condensation. A mass flow controller regulated flow through the cartridges. We kept cartridges refrigerated to the manufacturer-recommended temperature of <4°C before and after sampling until analysis was completed. Care was taken to minimize any particulate contaminates on the cartridge and sample container during handling and collection.

3.4.11. Exhaust Flow Measurement

We measured exhaust flow with the Ecom analyzer's pitot tube-based flow measurement probe. In most cases, we affixed the probe at the exhaust stack outlet during the entire period of gas sampling. In some cases, we held the probe for at least one minute at the stack outflow to collect the measurement.

3.5. Laboratory Analyses

3.5.1. Dilution of Sample Canisters

After sampling, we diluted fuel gas and exhaust gas sample canisters in the laboratory with ultrapure nitrogen gas to bring the concentrations of organic compounds within them into the range of our gas chromatography-mass spectrometry (GC-MS) system.

3.5.1.1. Fuel Gas Samples

We diluted fuel gas samples by attaching a PFA Teflon line to one end of the sample canister, slightly opening the canister valve to allow a flow of sample gas, waiting 30 seconds, withdrawing a quantity of gas from the PFA line with a syringe, and injecting the gas into a nitrogen stream generated by an Entech 4600 dynamic diluter. The flow from the diluter passed into an evacuated silonite-coated 6 L stainless steel canister. The diluter tracked the volume of nitrogen added to the canister, and we determined the dilution ratio from the volume of sample injected and the volume of nitrogen added. We then analyzed the contents of the diluted 6 L sample canister by GC-MS (Section 3.5.2). The fuel gas samples were diluted to an average of 2.50×10^{-3}% of their original concentrations.

3.5.1.2. Exhaust Gas Samples

We diluted some exhaust gas canister samples by the method described in Section 3.5.1.1, except that we first pressurized the samples to 3800 mbar with ultrapure nitrogen. Alternatively, we pressurized some exhaust gas samples to 3800 mbar and then diluted them with ultrapure nitrogen using the Entech 4600 dynamic diluter. Exhaust gas samples were diluted to an average of 3.00×10^{-2}% of their original concentrations.

3.5.1.3. Correction Using Methane Concentration Ratio

After analyzing the contents of canisters for non-methane hydrocarbons and alcohols with the GC-MS system (Section 3.5.2), we analyzed them with an LGR UGGA methane analyzer. We connected a PTFE Teflon-lined pump to each canister, and the pump pulled air from the canister and pushed it into a tee. One outlet of the tee vented to the atmosphere and the other was connected to the analyzer. In this way, the analyzer could experience canister air at near-atmospheric pressure, even as the pressure in the canister itself varied during sampling.

The methane concentration in each diluted canister divided by the concentration measured in exhaust gas during field measurements constituted an independent estimate of the dilution amount for each canister sample. We used this value to determine the original concentration of non-methane organic compounds in the exhaust gas.

3.5.2. Analysis of Non-methane Hydrocarbons and Alcohols

We analyzed canisters containing diluted fuel gas and exhaust gas samples for a suite of 55 hydrocarbons and three alcohols (see the list of compounds in Table 3-2). We used an Entech 7200

preconcentrator (in cold trap dehydration mode) and 7016D autosampler to concentrate samples and introduce them to a gas chromatograph (GC) system for analysis. The GC system consisted of two Shimadzu GC-2010 GCs, one with a flame ionization detector (FID) and another with a Shimadzu QP2010 Mass Spectrometer (MS). The FID detected C2 and C3 compounds, and the MS detected all other compounds. Details about the method were reported by Lyman et al. (2021a).

Table 3-2. List of organic compounds analyzed for this project. Compound group and analytical method are also shown for each compound.

Compound	Compound Group	Analytical method
Methane	Methane	LGR analyzer
Ethane	Alkane	GC-MS
Ethylene	Alkene	GC-MS
Propane	Alkane	GC-MS
Propylene	Alkene	GC-MS
Isobutane	Alkane	GC-MS
n-Butane	Alkane	GC-MS
Acetylene	Alkyne	GC-MS
Trans-2-butene	Alkene	GC-MS
1-Butene	Alkene	GC-MS
Cis-2-butene	Alkene	GC-MS
Isopentane	Alkene	GC-MS
N-Pentane	Alkane	GC-MS
Trans-2-pentene	Alkene	GC-MS
1-Pentene	Alkene	GC-MS
Cis-2-pentene	Alkene	GC-MS
2,2-Dimethylbutane	Alkane	GC-MS
Cyclopentane	Alkane	GC-MS
2,3-Dimethylbutane	Alkane	GC-MS
2-Methylpentane	Alkane	GC-MS
3-Methylpentane	Alkane	GC-MS
Isoprene	Alkene	GC-MS
1-Hexene	Alkene	GC-MS
n-Hexane	Alkane	GC-MS
Methylcyclopentane	Alkane	GC-MS
2,4-Dimethylpentane	Alkane	GC-MS
Benzene	Aromatic	GC-MS
Cyclohexane	Alkane	GC-MS
2-Methylhexane	Alkane	GC-MS
2,3-Dimethylpentane	Alkane	GC-MS
3-Methylhexane	Alkane	GC-MS

Compound	Compound Group	Analytical method
2,2,4-Trimethylpentane	Alkane	GC-MS
n-Heptane	Alkane	GC-MS
Methylcyclohexane	Alkane	GC-MS
2,3,4-Trimethylpentane	Alkane	GC-MS
Toluene	Aromatic	GC-MS
2-Methylheptane	Alkane	GC-MS
3-Methylheptane	Alkane	GC-MS
n-Octane	Alkane	GC-MS
Ethylbenzene	Aromatic	GC-MS
m/p-Xylene	Aromatic	GC-MS
Styrene	Alkene	GC-MS
o-Xylene	Aromatic	GC-MS
n-Nonane	Alkane	GC-MS
Isopropylbenzene	Aromatic	GC-MS
n-Propylbenzene	Aromatic	GC-MS
1-Ethyl-3-methylbenzene	Aromatic	GC-MS
1-Ethyl-4-methylbenzene	Aromatic	GC-MS
1,3,5-Trimethylbenzene	Aromatic	GC-MS
1-Ethyl-2-methylbenzene	Aromatic	GC-MS
1,2,4-Trimethylbenzene	Aromatic	GC-MS
n-Decane	Alkane	GC-MS
1,2,3-Trimethylbenzene	Aromatic	GC-MS
1,3-Diethylbenzene	Aromatic	GC-MS
1,4-Diethylbenzene	Aromatic	GC-MS
Methanol	Alcohol	GC-MS
Ethanol	Alcohol	GC-MS
Isopropanol	Alcohol	GC-MS
Formaldehyde	Carbonyl	HPLC
Acetaldehyde	Carbonyl	HPLC
Acrolein	Carbonyl	HPLC
Acetone	Carbonyl	HPLC
Propionaldehyde	Carbonyl	HPLC
Crotonaldehyde	Carbonyl	HPLC
Butyraldehyde	Carbonyl	HPLC
Methacrolein	Carbonyl	HPLC
2-Butanone	Carbonyl	HPLC
Benzaldehyde	Carbonyl	HPLC
Valeraldehyde	Carbonyl	HPLC

Compound	Compound Group	Analytical method
Tolualdehyde	Carbonyl	HPLC
Hexaldehyde	Carbonyl	HPLC

3.5.3. Analysis of Carbonyls

We eluted and analyzed DNPH cartridges by modifications of the methods of Uchiyama et al. (2009), Anneken et al. (2015), Shimadzu method LAAN-J-LC-E090 (Shimadzu, 2011), and Restek Lit. Cat.# EVSS2393A-UNV (Restek, 2018). These techniques are somewhat different from EPA Method TO-11A (EPA, 1999), which has become outdated due to improved instrumentation capabilities. We kept used and unused cartridges refrigerated or on ice, except when installed for sampling. We eluted cartridges within 14 days of sampling and analyzed the eluent within 30 days. To elute DNPH cartridge samples, we flushed cartridges with a 5 mL solution of 75% acetonitrile and 25% dimethyl sulfoxide. We collected the solution into 5 mL volumetric flasks and brought the flasks to a volume of 5ml using 0.5-1 mL of the acetonitrile/dimethyl sulfoxide solution. Finally, we pipetted a 1.6mL aliquot from the 5 mL flask into two 2 mL autosampler vial for analysis by High Performance Liquid Chromatography (HPLC). The second vial was kept as a spare in case of contamination or equipment failure in the lab.

We used a commercial standard mixture (AccuStandard M-1004) of derivatized aldehydes in acetonitrile to develop the calibration curve. We analyzed samples with a Shimadzu Nexera-i LC-2040C 3d Plus HPLC and a Shimadzu Shim-Pack Velox C18 column. We used a mixture of acetonitrile, tetrahydrofuran, and water as the eluent. We calibrated the instrument on each analysis day with a five-point calibration curve. We ran at least one additional calibration standard at the beginning and end of each analysis batch to check for retention time drift or other errors.

3.6. Calculation of Emission Rates and Air-fuel Ratio

To calculate the emission rate for each compound, we first multiplied the measured exhaust velocity (m s^{-1}) by the cross-sectional area of the stack (m^2) at its exit to determine the flow rate of the exhausted gas (m^3 s^{-1}). We then multiplied this flow rate by the concentration of each measured compound (g m^3) to determine the emission rate of the compound (g s^{-1}). All compounds except carbonyls were measured as mixing ratios (units of parts-per-billion by volume, or ppb). We converted mixing ratios to density units (g m^3) for emission rate calculations at standard conditions of 25°C and one atmosphere. Before calculating emission rates, we converted measured volumetric flow rates to standard flow using these same conditions.

We calculated the air-fuel ratio of each engine using the Brettschneider equation (Brettschneider, 1979).

3.7. Quality Assurance

3.7.1. Flow Rates

We compared the Ecom pitot tube against a recently factory-calibrated Pacer DA400 rotating vane anemometer. Because of the bidirectional nature of engine exhaust flow, rotating vane anemometers are not useful for exhaust measurements. We performed the comparison using a 20 cm duct and a blower to generate airflow, and we partially blocked the duct intake to vary the flow between 2 and 6 m s^{-1}. The difference between the two instruments was 5.3 (3.9, 6.9)%.

As another way of checking our data, we compared measured volumetric flow rates of engine exhaust against the flow rate calculated by multiplying the rotations per minute (RPMs) of the engine by the displacement volume of its cylinder(s). Calculation of the flow rate from RPMs and displacement volume is admittedly coarse, especially since our measurement method for RPMs was to count the rotation aurally. It does provide a way of assuring that our measured flow rates were within a reasonable range, however. Figure 3-1 shows that the two methods agree to within a few m^3 min^{-1} in most cases.

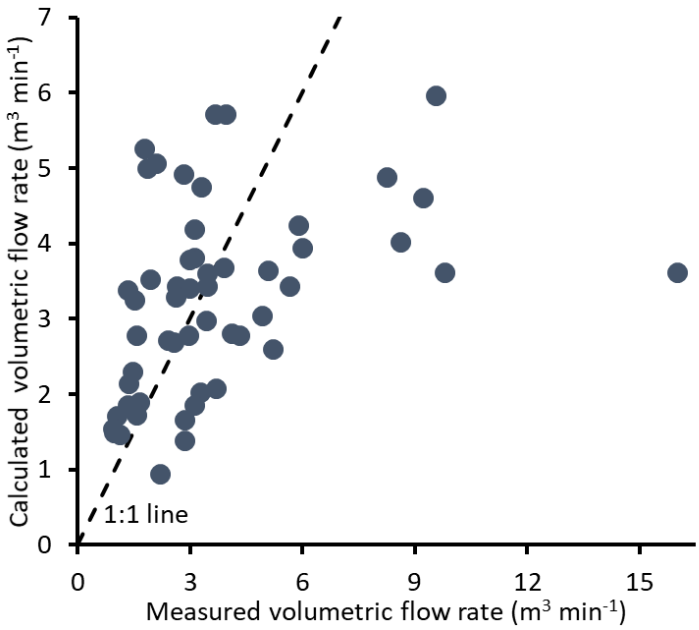

Figure 3-1. Measured volumetric flow rate of engine exhaust versus the flow rate calculated from RPMs and engine cylinder displacement volumes.

The pitot tube should be inserted perpendicular to the exhaust flow, with one of the holes to measure differential pressure facing the flow direction, and the other facing against the flow direction. We were inconsistent in orientation of the pitot tube throughout the campaign. Orientation impacted flow rates by as much as 44%. We corrected pitot tube flow measurements for orientation when needed.

3.7.2. Inorganics

We performed weekly calibration checks of the Ecom instrument's recovery of NO, NO_2, CO, CO_2, and O_2 in our laboratory with compressed gas standards by inserting the instrument's sampling inlet into a 3 cm diameter tube and flooding the tube with calibration gas. We also had the instrument calibrated at the factory semiannually. Calibration checks in air free of the measured gases produced responses of zero in all cases. The recovery of non-zero concentrations of the measured gases is shown in Table 3-3.

Table 3-3. Calibration recovery for NO, NO_2, CO, CO_2, and O_2 by the Ecom analyzer.

Gas	Percent recovery
NO	100 (97, 102)
NO_2	83 (77, 90)
CO	98 (94, 103)
CO_2	100 (98, 101)
O_2	100 (100, 100)

3.7.3. Methane

3.7.3.1. Field Methane Measurements

We calibrated the methane analyzer at a minimum of two points along its measurement range, including one zero point, on each field measurement day. We performed calibrations with four non-zero points weekly. We used a custom-built scrubber system to generate methane and carbon dioxide-free air, and we diluted NIST-traceable compressed gas standards with calibrated mass flow controllers for span calibrations. Calibration zero points were 1 (0, 2) ppb. The analyzer has two lasers for methane, one for 0-2000 ppm, and one for concentrations greater than 2000 ppm. Calibration recovery was 105 (104, 107) and 98 (96, 99)% for the low and high lasers, respectively.

3.7.3.2. Laboratory Methane Measurements

We calibrated the methane analyzer used to measure the methane concentration of sample canisters on each day of use using ultrapure nitrogen gas and NIST-traceable compressed gas standards. Calibration zero points were 1 (0, 1) ppb. Non-zero percent recovery was 100 (99, 101)%.

3.7.4. Non-methane Hydrocarbons (NMHC) and Alcohols

3.7.4.1. Matrix Spike Results for Hydrocarbons

We used a compressed natural gas standard (72% methane) to perform matrix spikes on the sampling system. We injected the gas standard into the sampling inlet at a known rate through a stainless steel tee, and we collected canister samples normally. We also collected samples directly from the standard cylinder to verify the composition of gas in the cylinder. We performed these tests during regular engine exhaust sampling in the field and while sampling ambient air at the USU laboratory. The results in Figure 3-2 show the recovery of compounds in the matrix spike samples.

In the figure, 100% recovery means that the total amount of all hydrocarbons measured with our emissions measurement system during matrix spikes was 100% of what we expected to measure, as calculated from the known composition of the natural gas standard and the flow rate of the standard into the system, and as corrected for concentrations of each compound in samples collected under the same conditions but without natural gas standard added. Values in the figure greater than 100% mean that we measured more hydrocarbons than expected during matrix spikes, and values less than 100% mean the opposite.

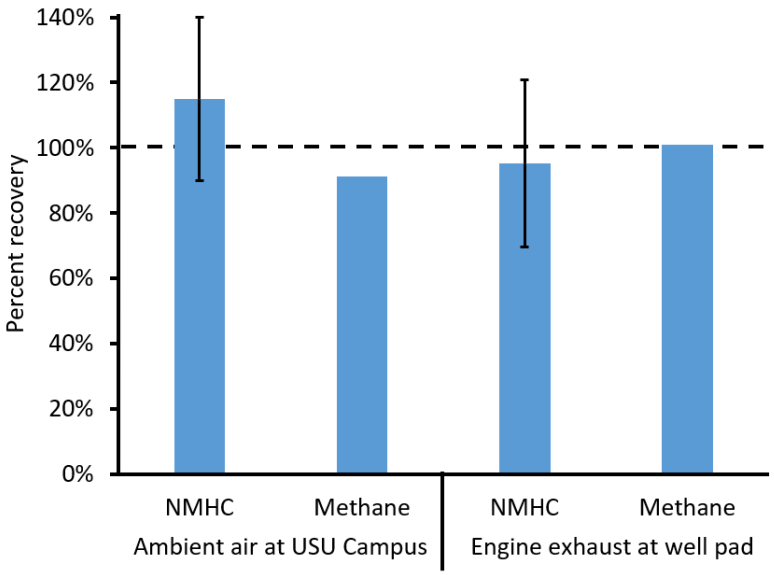

Figure 3-2. Recovery of hydrocarbons by the emissions measurement system. n = 2 for the USU campus results and the engine exhaust results. Whiskers show 95% confidence intervals calculated from results for individual NMHC compounds.

3.7.4.2. Laboratory Results

Duplicate analyses of canister samples were 0 (-2, 2)% different. Blanks contained 0.12 (0.11, 0.14) ppb of individual organic compounds. All results were blank-corrected. Recovery of calibration standards was 99 (99, 100)%.

3.7.5. Carbonyls

3.7.5.1. Matrix Spike Results

We used Dynacal permeation tubes containing formaldehyde and propionaldehyde in a Model 120 Dynacalibrator to perform matrix spike tests of carbonyls on the emissions measurement system. We connected the calibrator output to the inlet of the sampling line with a stainless steel tee and collected DNPH samples normally. We also attached DNPH cartridges directly to the Dynacalibrator output line for comparison against the matrix spike results. The results in Figure 3-3 show the percent recovery of formaldehyde and acetaldehyde passed through the entire sampling system compared to the amount collected directly from the output line.

We performed these tests in ambient air at the USU campus. We attempted to perform identical tests in the field while we measured emissions from an engine as we did for hydrocarbons in Section 3.7.4.1, but the pulsating pressure of the exhaust interfered with the flow of gas from the calibrator, leading to erratic measured flows. In the future, we plan to inject liquid standards containing carbonyl compounds as a matrix spike during engine sampling.

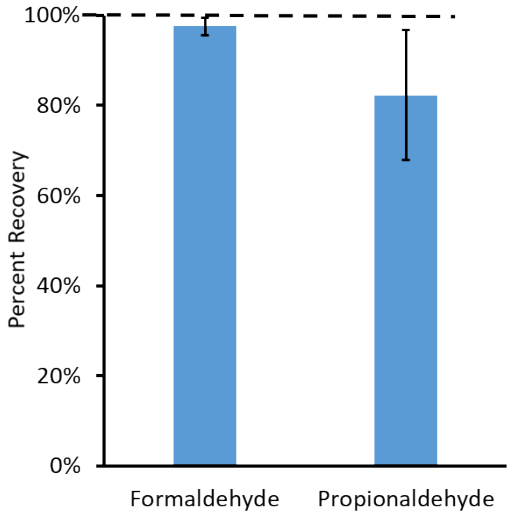

Figure 3-3. Recovery of carbonyls by the emissions measurement system when operated at the USU campus (n = 3). Whiskers show 95% confidence intervals.

3.7.5.2. Laboratory Results

Duplicate analyses of canister samples were 14 (10, 23)% different. Blanks contained 0.02 (0.01, 0.0.02) ppb of individual carbonyl compounds. All results were blank-corrected. Recovery of calibration standards was 100 (99, 102)%.

3.7.5.3. Overloading of Some DNPH Cartridges

The cartridges used to collect carbonyls from exhaust gas were filled with amorphous silica beads coated with acidified DNPH. Carbonyls bind to DNPH and become entrapped by the cartridge as gas passes through it. Upon analysis in the laboratory, we identified some cartridges that were overloaded with carbonyls, as indicated by the absence of a DNPH peak in the chromatogram (i.e., all the DNPH had been used) and by an equal concentration of carbonyl compounds on both DNPH cartridges that were placed in the flow path in series (i.e., the first and second cartridges had both become completely loaded). Carbonyl data for these samples can be considered a lower limit of the actual carbonyl concentration. Samples with overloaded DNPH cartridges are indicated in the final dataset and were not used for analyses of organic compound composition.

3.7.6. Correction of Chemical Measurements Based on Depth of Probe in Stack

Engine exhaust flows are bidirectional (Nakamura et al., 2005), leading to the entrainment of ambient air into the exhaust stack. Thus, probes that pull gas samples from the stack must be inserted far

enough to avoid contamination from ambient air. We performed tests of the influence of probe depth on five engines (Figure 3-4). For the figure, we normalized the average concentrations of CO, NO, CO_2, and the inverse of O_2 at each sampling depth. We found that depths of less than about 1 m resulted in contamination from ambient air and reduced recovery. The majority of stacks we encountered were long enough for us to insert our sample probes to depths of 1 m or more. In some cases, stacks were as short as 0.3 m or mufflers impeded probe entry even though the stack was 1 m or longer. We used the results shown in the figure to derive a polynomial regression equation and used that equation to correct chemical measurements collected at less than 1 m.

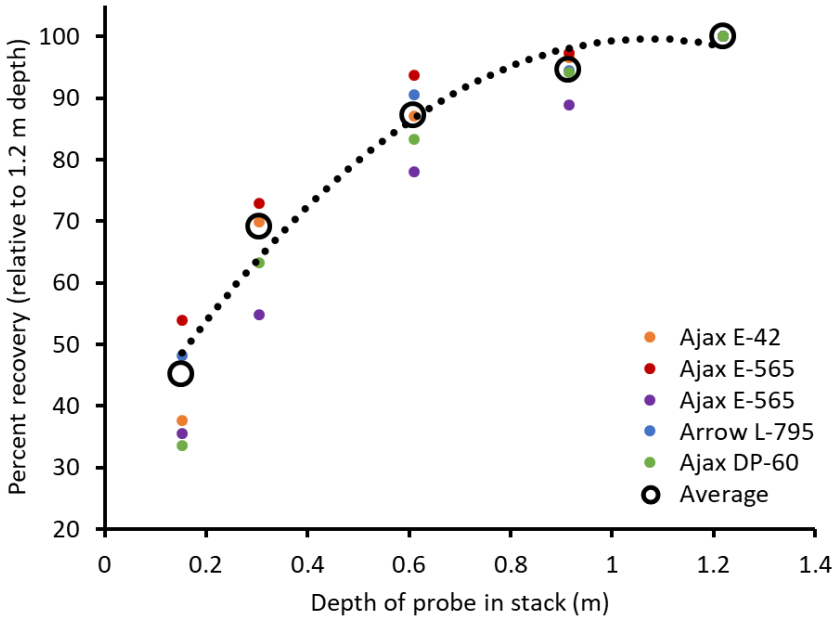

Figure 3-4. Relative recovery of inorganic compounds versus depth of sampling probe in the stack. Colors indicate measurements from individual engines. Open black circles represent averages. The dotted line is the regression curve used to correct measurements collected from probes less than 1.2 m within the stack.

3.7.7. Comparison Against Other Methods

3.7.7.1. Calculation of NO_X Emissions Using Engineering Equations

For this study, we measured emission rates directly from gas concentrations and exhaust gas flow rates (see Section 0). Some protocols allow for estimation of emission rates from exhaust gas concentrations alone via engineering equations. We compared our measurements against the engineering equation recommended by the State of Wyoming (equation in Section 10.1.2 of DEQ (2006)). The equation uses concentrations of NO_X and O_2 to determine the emission rate of NO_X in g hp^{-1} h^{-1}. We used our measured NO_X and O_2 data in the equation, and we divided our NO_X emission results obtained as described in Section 0 by horsepower to obtain equivalent units for comparison. We used the rated horsepower of each engine as a proxy for the actual measured horsepower, which is almost certainly an overestimate for many of the engines, and can be expected to lead to an underestimate of g hp^{-1} h^{-1}. For a subset of engines from one company, the company used site-specific dynamometer-measured load data to calculate actual engine horsepower. Horsepower calculated from these load

measurements tended to be lower than the rated engine horsepower. Figure 3-5 shows a comparison of these methods.

Most of the values in Figure 3-5 fall near the 1:1 line, except for the six blue circles with orange centers shown in the figure. Engineering equation NO_X emissions were at least 1.5 g hp^{-1} h^{-1} greater than directly measured NO_X emissions in those six cases. Those six cases tended to have higher NO_X concentrations in exhaust gas than the remaining samples (797 (335, 1609) ppm versus 35 (21, 68) ppm). It is possible that the engineering equation overestimates NO_X emissions when exhaust gas contains very high NO_X concentrations. With those six cases excluded, the engineering equation method produced 0.12 (0.09, 0.18) g hp^{-1} h^{-1} more NO_X emissions than the direct measurement method. Use of horsepower calculated from dynamometer data at engines for which the data were available, rather than engine-rated horsepower in the direct measurement method, led to 1.5 (1.3, 1.7) times higher NO_X emissions per horsepower.

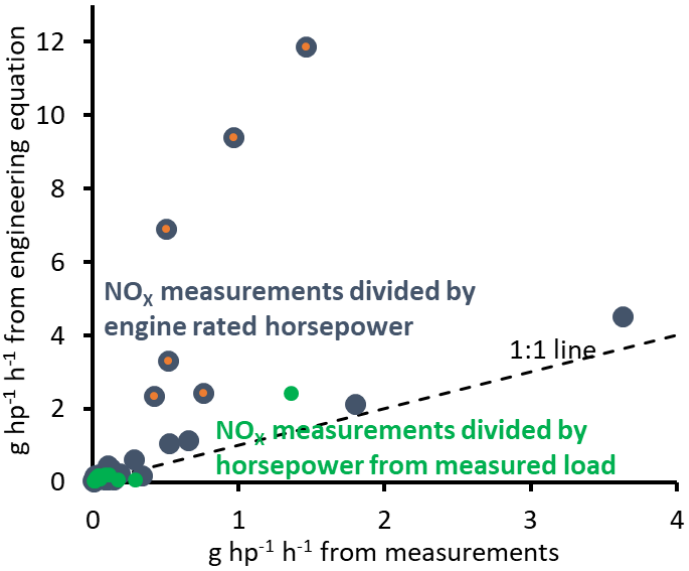

Figure 3-5. Comparison of NO_X emissions per horsepower from emission rate measurements against values calculated from an engineering equation. X-axis values for the blue-gray circles were determined by dividing NO_X measurements by engine-rated horsepower. X-axis values for the green circles were determined by dividing NO_X measurements by horsepower calculated from dynamometer measurements, and are only available for a subset of samples. Blue-gray circles with orange centers are discussed in the text.

3.7.7.2. Comparison Against Existing Concentration Data

Figure 3-5 compares two different methods of calculating NO_X emissions from the same exhaust gas concentration data. We also obtained emissions test results from a company for two Ajax E42 engines, one Ajax E565, and one Arrow L795. These measurements were collected by a consulting company using protocols specified in EPA 40 CFR 60 (CFR, 2021). They measured emissions from each of the engines four times, with the fuel valve in a different position each time. We compared concentrations of pollutants measured in the consulting company's dataset to those in our dataset. We only used data

from this study that were within the range of O_2 measurements from the consultant dataset in the comparison. The results of this comparison are in Table 3-4.

Regulatory protocol measurements (including those used in this comparison) use flame ionization detection (FID) to determine hydrocarbon concentrations, and the instruments are calibrated with propane. FID detectors are sensitive to the number of carbons in a compound, so 1 ppm of propane (with three carbons per molecule) results in about three times the signal as 1 ppm of methane (with one carbon per molecule). Thus, the methane component of the instrument signal can be expected to be under-counted by three times. The consultant dataset we used reported total hydrocarbons (THC) and non-methane hydrocarbons (NMHC). To calculate methane concentrations equivalent to our measurements, we multiplied THC and NMHC by three, and then we subtracted NMHC from THC. To compare our measurements against NMHC data from the consultant dataset, we multiplied our compound-specific hydrocarbon values by the number of carbons in each compound and divided those values by three.

Table 3-4. Comparison of gas concentrations measured in engine exhaust in this study against those measured by a consulting company following EPA regulatory protocols. Data from this study that fall outside the range of O_2% in the consultant dataset are excluded. Values in parentheses are lower and upper 95% confidence limits.

Gas	USU average	Consultant dataset average	P-value of t-test to determine difference
NO_X (ppm)	66.3 (30.1, 140.3)	88.6 (54.8, 185.0)	0.56
CO (ppm)	4441 (2216, 8142)	1387 (728, 2331)	0.06
Methane (ppm)	18150 (14408, 22572)	16210 (13812, 18526)	0.43
NMHC (as propane; ppm)	2397 (1890, 3014)	1209 (1015, 1445)	<0.01

Table 3-4 shows statistically similar values for the two datasets for NO_X, CO, and methane, but higher values for NMHC. CO is higher in the USU dataset, but not significantly, using $\alpha = 0.05$. Differences in methodology may account for the NMHC difference. On the other hand, the consultant dataset only comprises four engines, and a larger comparison may yield different results.

4. Deviations

The project deviated from its original aims in the following ways:

1. We intended to collect all measurements during the winter season, but it took longer than anticipated for an adequate number of companies to agree to participate in the study, so we ultimately collected samples between January and May 2021. To determine whether engine emissions were meaningfully different in summer versus winter, in January 2022 we measured emissions from five engines we originally measured in May. The results of those tests are in Section 5.5.
2. We planned to measure the impact of engine operating characteristics (fuel intake, oil injection rate, air intake) on emissions, but this work was not able to be performed because of cost limitations and difficulty finding willing partners.

5. Results

5.1. Differences Among Engine Types

The different types of engines we encountered had different magnitudes and compositions of pollutant emissions (Figure 5-1 and Figure 5-2) In general, Ajax engines tended to have higher total emissions and higher variability than Arrow engines. Ajax engines also tended to have more organic compound emissions as a percentage of the total. We only measured two GM Vortec engines, but they had very low CO and organic compound emissions and the highest emissions of NO_X. The GM Vortec engines were the only four-stroke engines measured.

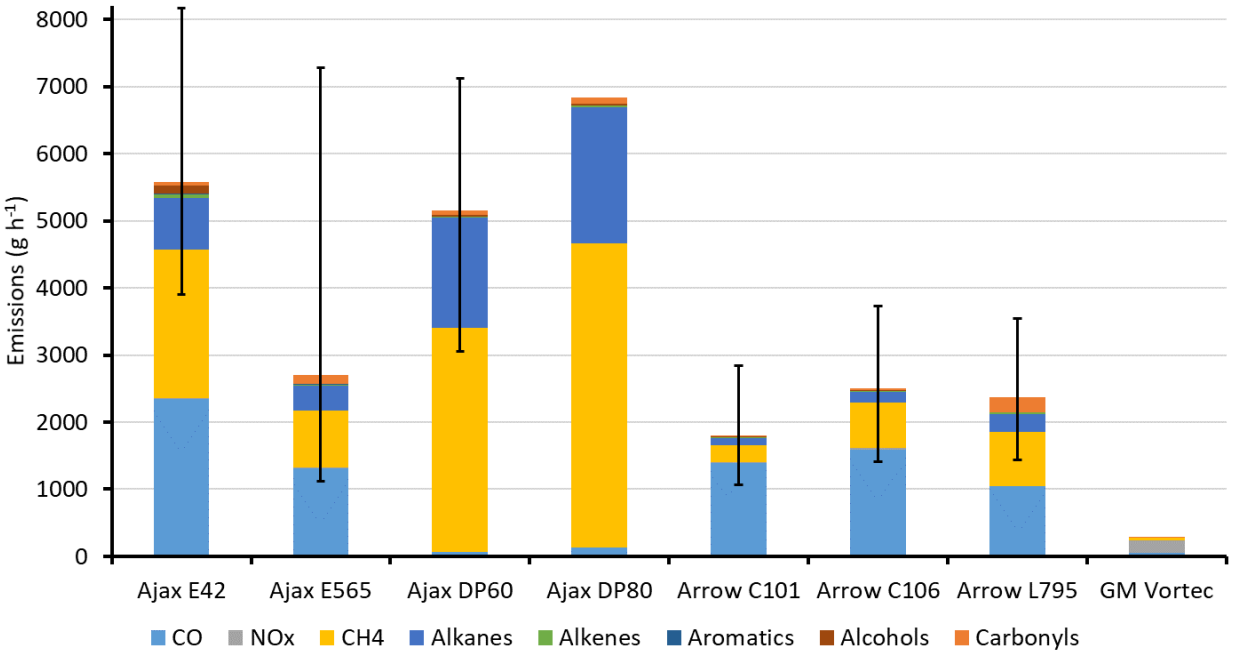

Figure 5-1. Emissions of pollutant gases from the engine makes and models shown. The top of the bar is the average total emission, and the whiskers show bootstrapped 95% confidence intervals. The colored sections of the bars show emissions of the compounds or compound groups indicated.

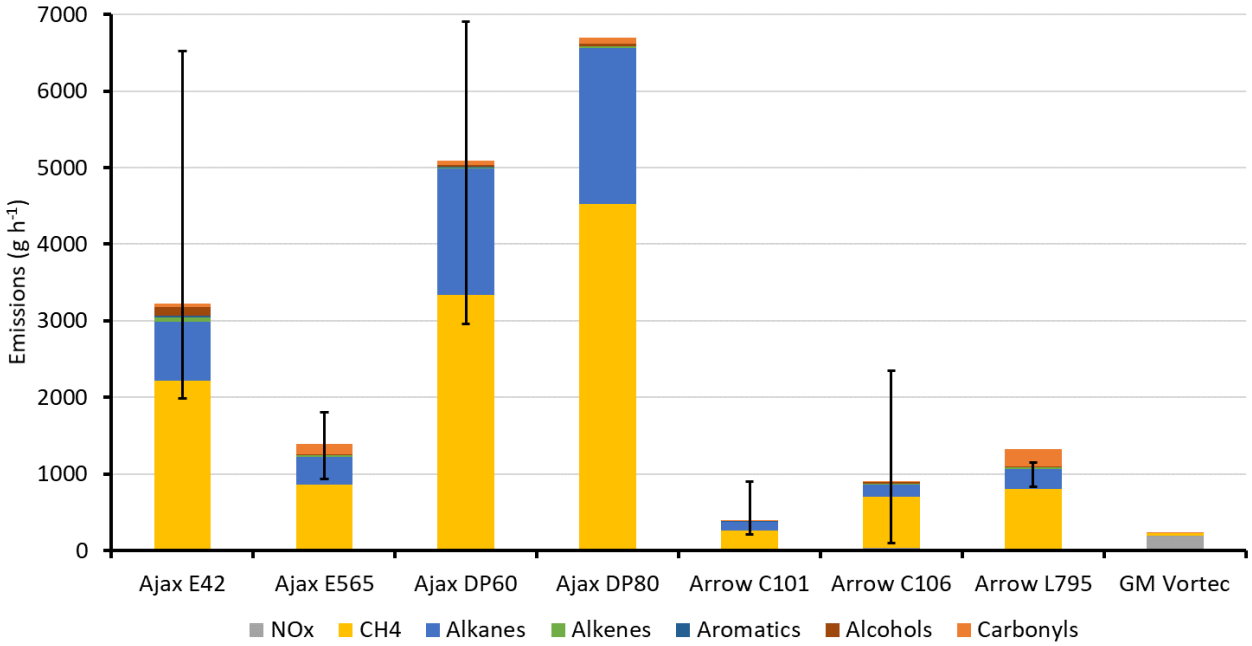

Figure 5-2. Same as Figure 5-1, except that CO is excluded.

5.2. Influence of Air-fuel Ratio

Many characteristics of engine emissions in the study were correlated with the engine air-fuel ratio (also called lambda). An engine's air-fuel ratio is the ratio of air in the engine's combustion chamber to the amount of air needed for combustion of the fuel. Stoichiometric combustion, with an air-fuel ratio of one, has exactly the amount of oxygen needed to combust the available fuel. In general, engines with an air-fuel ratio near one tend to burn hotter, which causes them to produce and emit more NO_X. Engines with air-fuel ratios less than one (also called rich burn) or greater than one (also called lean burn) are cooler, resulting in less NO_X (Wang et al., 2019). Rich burn engines tend to produce more CO because not enough O_2 is available to facilitate complete combustion. Lean burn engines produce less CO, CO_2, and NO_X. These relationships between air-fuel ratio and exhaust characteristics were present in the data we collected (Figure 5-3 and Figure 5-4).

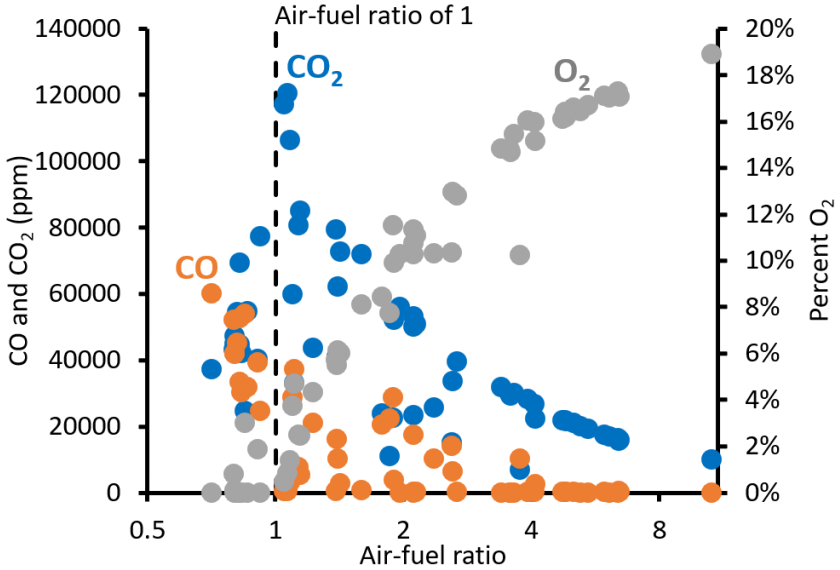

Figure 5-3. Concentrations of O_2, CO, and CO_2 measured in exhaust gas versus the air-fuel ratio of the engine. The x-axis is in log scale.

Figure 5-4 shows that, as expected, lower air-fuel ratios were associated with higher NO_X concentrations in the exhaust gas, up to an air-fuel ratio of one, and then at air-fuel ratios less than one, NO_X tended to decrease again ($r^2 = 0.36$ for the relationship between air-fuel ratio and NO_X). NO_X tended to be especially low, usually less than 10 ppm, at air-fuel ratios greater than three.

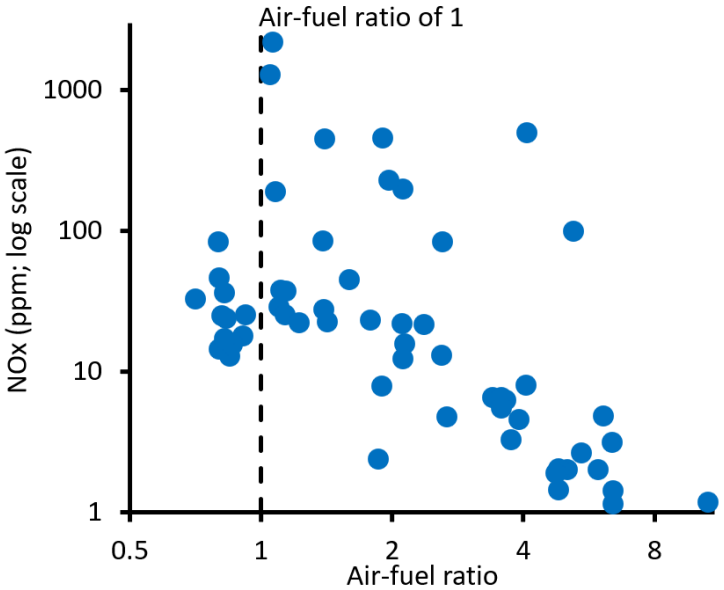

Figure 5-4. Concentration of NO_X in exhaust gas versus engine air-fuel ratio. The x- and y-axes are in log scale.

Figure 5-5 shows that more NO existed relative to NO_2 in exhaust gases with higher total NO_X ($r^2 = 0.73$). Another way to think about this is that a somewhat consistent amount of NO_2 existed in all exhausts

sampled, while the NO concentration was higher at higher total NO_X concentrations. Thus, lean burn engines (with high air-fuel ratio and low NO_X) tended to have more NO_2 as a percentage of total NO_X.

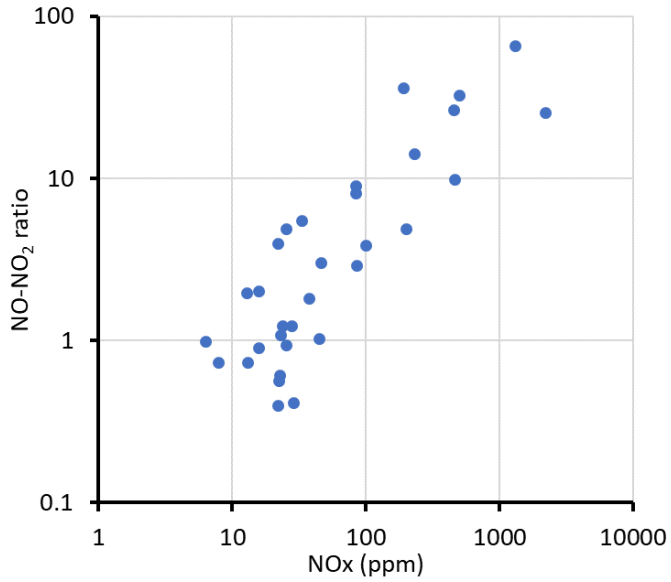

Figure 5-5. Ratio of the concentration of NO to NO_2 versus the NO_X concentration in the exhaust gas. Both axes are in log scale.

The fuel for these engines was natural gas, which contains organic compounds composed mostly of carbon and hydrogen. Complete combustion converts those organic compounds to CO_2. They may also be converted to CO, soot, or other organic compounds, especially alkenes, alkynes, and carbonyls. For this section, however, we consider combustion more simply to be the conversion of organic compounds in fuel to CO or CO_2, and we calculate combustion completeness as one minus the percent of carbon atoms in exhaust gas associated with organic compounds versus the total number of carbon atoms in the gas. By this method, 80% combustion completeness means that 80% of carbon atoms introduced as fuel gas were combusted to CO or CO_2, while the remaining 20% were still in organic form when exhausted. Figure 5-6 shows that the combustion completeness of measured engines depended on the air-fuel ratio, with completeness decreasing at higher air-fuel ratios ($r^2 = 0.62$). For engines with air-fuel ratios greater than three, combustion was less than 50% complete on average. In other words, less than 50% of the carbon atoms in the fuel gas were combusted to CO or CO2, and more than 50% of the carbon in the fuel was released into the atmosphere as organic compounds. Fuel that passes through the engine uncombusted is also called fuel slip (Kuppa et al., 2019).

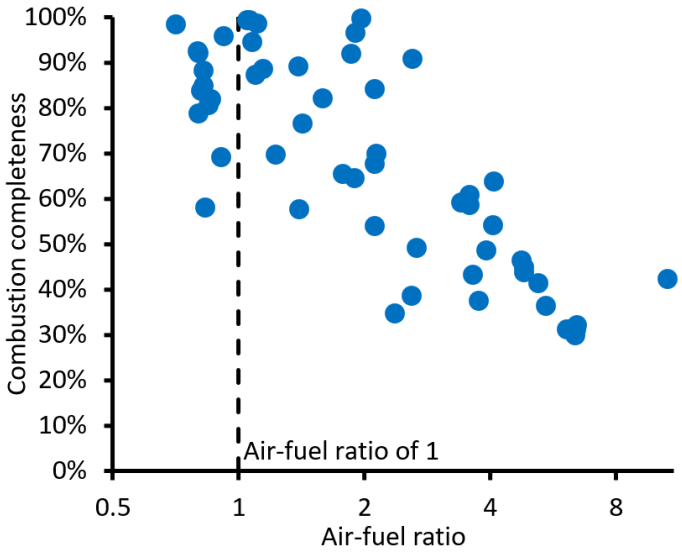

Figure 5-6. Percent combustion completeness versus the air-fuel ratio of the engine. The x-axis is in log scale.

While engines with higher air-fuel ratios tended to exhaust more fuel, engines with lower air-fuel ratios tended to emit a larger percentage of their fuel as reactive organic compounds, including carbonyls and alkenes. Figure 5-7 shows that carbonyls and alkenes+acetylene tended to increase as air-fuel ratios decreased. Exhaust from engines with air-fuel ratios greater than three had the lowest concentrations of these compounds.

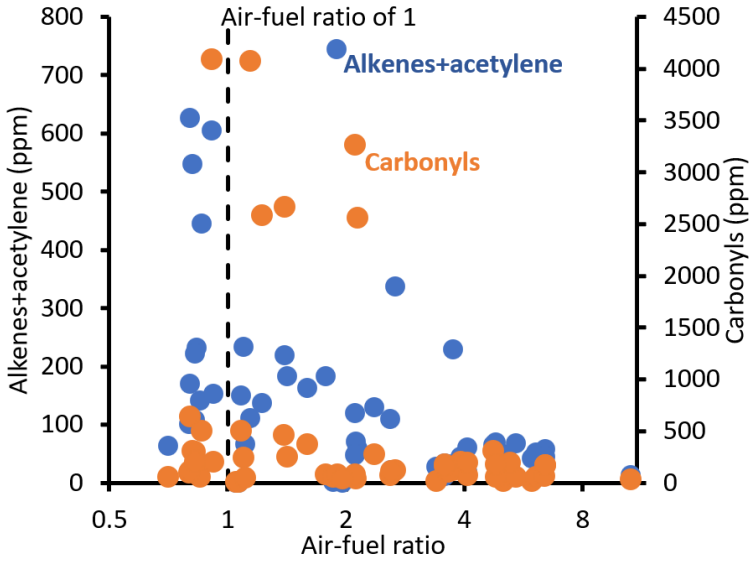

Figure 5-7. Concentrations of alkenes+acetylene and carbonyls versus air-fuel ratio. The x-axis is in log scale.

To summarize, air-fuel ratios greater than one, and especially those greater than three, led to lower NO_X and lower combustion completeness (i.e., higher organic compound emissions), while lower air-fuel

ratios led to higher NO_X, higher combustion completeness, and higher emissions of reactive organics. Figure 5-8 summarizes these characteristics for each engine type measured.

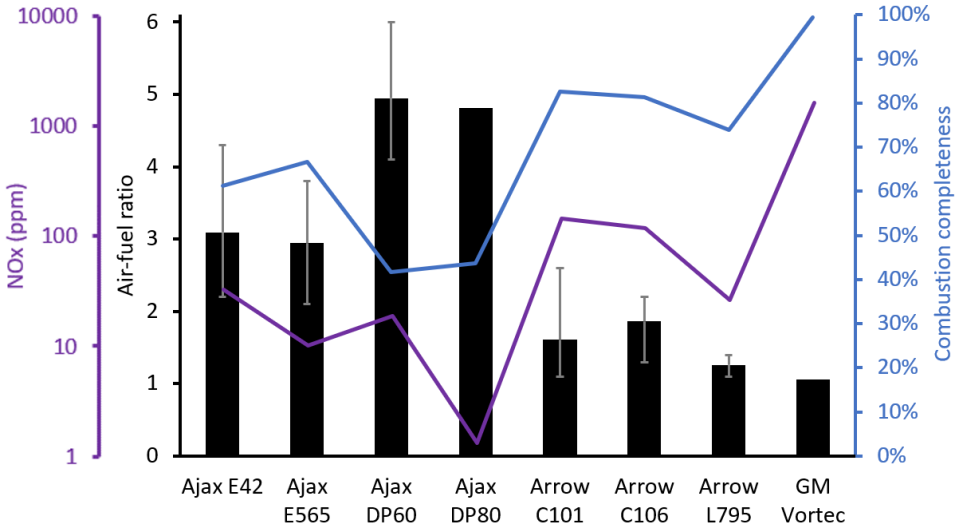

Figure 5-8. Average air-fuel ratio, NO_X concentrations, and combustion completeness for each type of engine measured in this study. Black bars show the average air-fuel ratio, and grey whiskers show the 95% confidence interval of the air-fuel ratio. The purple and blue lines show NO_X and combustion completeness, respectively, for each engine type.

5.3. Organic Compound Composition

Figure 5-9 and Figure 5-10 show the composition of organic compounds in fuel gas and exhaust gas samples. Exhaust gas was richer in alkenes and acetylene than fuel gas (Figure 5-9). We did not measure carbonyl concentrations in fuel gas, but previous studies have shown them to be very low (Lyman and Tran, 2015; Wilson et al., 2020), especially when compared to the concentrations in exhaust gas. Figure 5-9 shows that emissions in this study contained more methane and fewer alkenes than in a profile from the EPA SPECIATE database that is used by photochemical modelers to represent emissions from natural gas-fueled pumpjack engines.

Figure 5-9 and Figure 5-10 show the average composition of fuel gas used by each company. Companies A and C used gas that had been transported from the well pad, processed, and then returned to the pad for use as fuel, whereas Company B used as fuel unprocessed gas produced at the well pad.

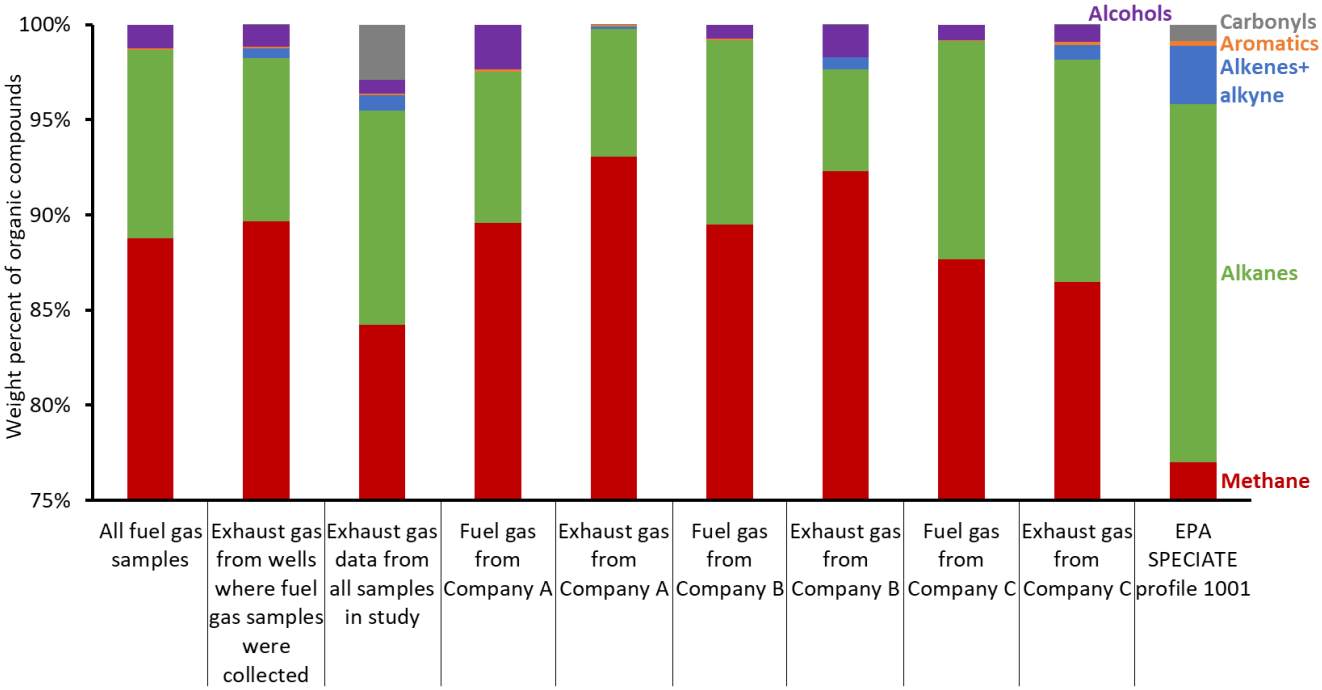

Figure 5-9. Composition of organic compounds by compound group in fuel gas and exhaust gas samples and an emissions profile from the EPA SPECIATE database.

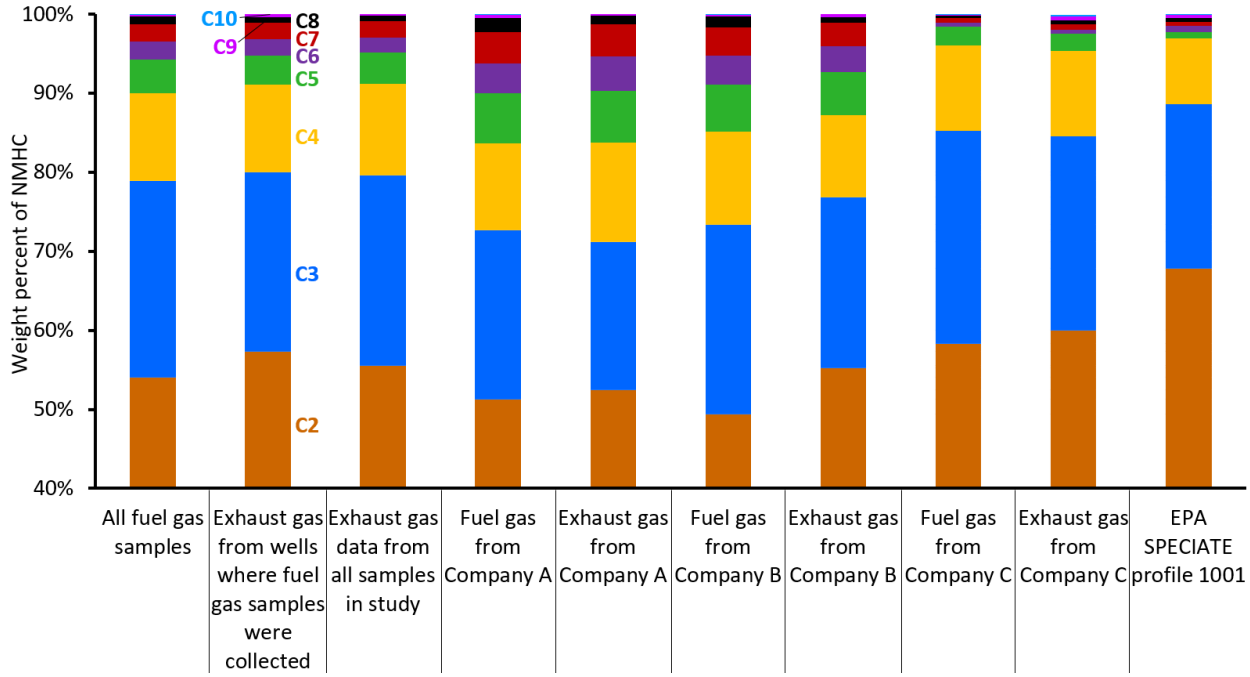

Figure 5-10. Composition of hydrocarbons by carbon number in fuel gas and exhaust gas samples and an emissions profile from the EPA SPECIATE database.

5.4. Pumping versus Idled engines

We sampled a subset of engines that were partially idled. These engines were powering glycol pumps to heat well equipment but were not powering pumpjacks. They showed lower emissions of CO_2 and NO_X relative to a set of engines of the same makes and models from the same operator and the same sampling period, but the differences were not statistically significant (Figure 5-11).

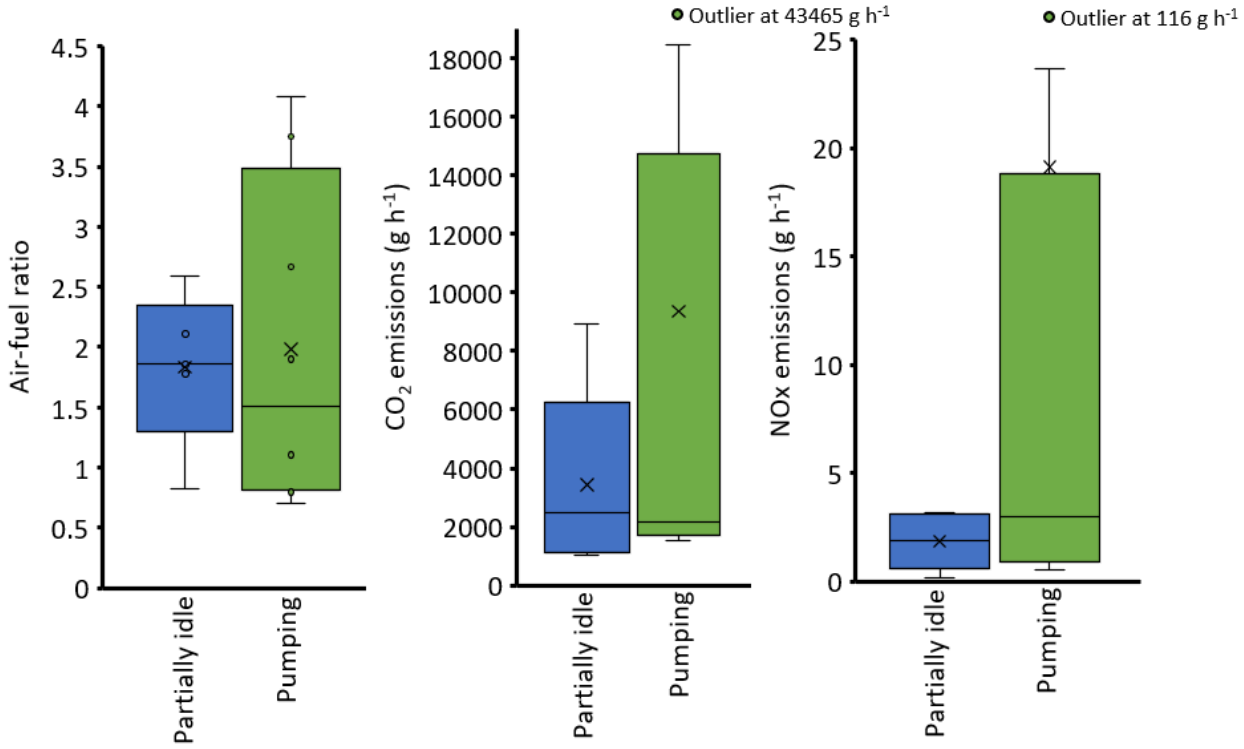

Figure 5-11. Box and whisker plots of a subset of engines that were partially idled compared to a set of equivalent engines that were powering pumpjacks. The tops and bottoms of boxes show 75 and 25 percentiles. Whiskers show minima and maxima. The x shows the mean, and the horizontal line in each box is the median.

5.5. Exhaust Stack Exit Temperatures

We found no meaningful correlations between the temperature at the exit of exhaust stacks and any other parameter. Exhaust stack lengths varied from about 0.5 m to more than 5 m and were of varying diameters and designs. When we only considered stacks of similar lengths, exhaust and ambient temperature had a significant relationship ($r^2 = 0.57$; Figure 5-12).

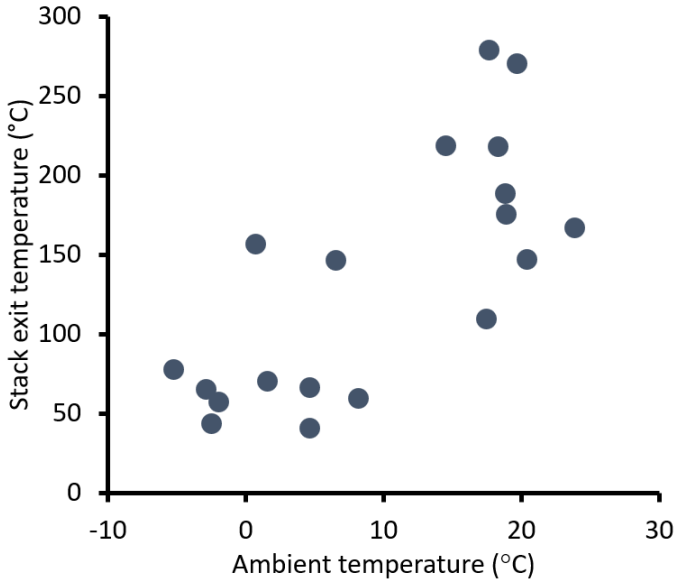

Figure 5-12. Ambient versus exhaust stack exit temperature for engines with exhaust stacks greater than 3 m in length.

Stack temperature and stack length were inversely related ($r^2 = 0.49$), as Figure 5-13 shows.

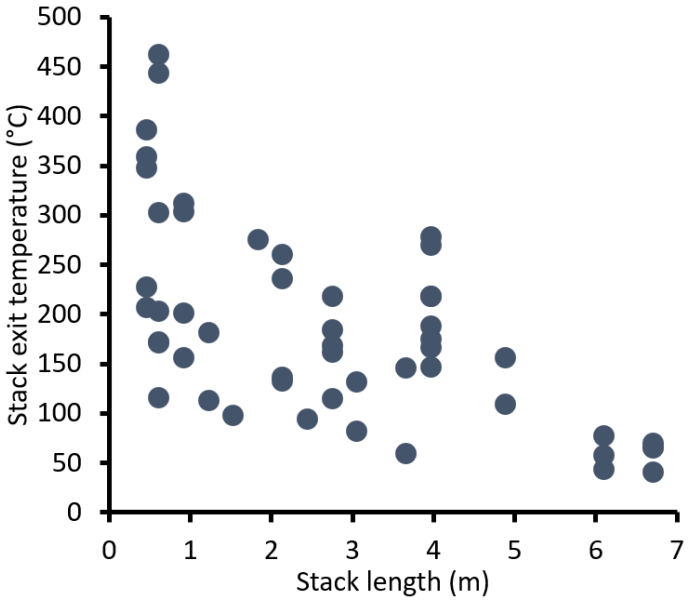

Figure 5-13. Exhaust stack length versus stack exit temperature.

We used the exponential relationship between stack exit temperature and stack length (Figure 5-13) to determine the expected stack temperature for a given length. We then determined the temperature residual for each engine by subtracting the actual temperature from the expected temperature. This temperature residual is a relative estimate of engine temperature. Engines with a high stack temperature residual likely burned hotter than those with a low residual. Figure 5-14 shows a weak

positive relationship of residual stack temperature with NO_X and combustion completeness (r^2 = 0.10 for both). These relationships likely occurred because hotter engine temperatures allowed more NO_X formation and more complete combustion. The relationships in Figure 5-14 are probably weak because of unaccounted-for influences from stack design, ambient temperature, engine type, and other variables. We also averaged combustion completeness and NO_X values in 50°C bins, such that all the data points that had stack temperature residuals between 50 and 100°C were averaged together, and so on. Not surprisingly, binned average combustion completeness and NO_X were better correlated with temperature residuals (r^2 = 0.66 and 0.46, respectively).

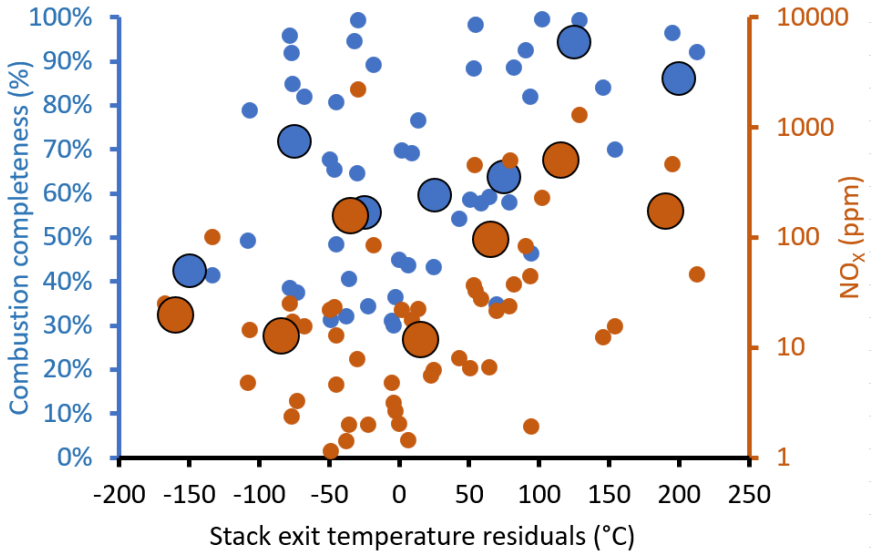

Figure 5-14. Concentrations of total organics and NO_X versus stack exit temperature residuals. Small dots show values from individual measurements, and large circles are averages for 50°C bins.

5.6. Other Exhaust Stack Characteristics

Of the 58 engines in the study, 49 (or 84% of the total) and 9 (16%) had horizontal and vertical stacks, respectively. Stack heights and stack inside diameters were fairly consistent across horizontal stacks 0.75 m and 0.1 m, respectively; Table 5-1). We observed strong variations in stack exit temperature and exhaust flow, with no clear difference in these values between lean burn and rich burn engines. Stack characteristics of vertical stacks varied more than horizontal stacks, but the sample size was small.

Note that stack parameters are provided for internal combustion engines in version 1.89 of the Utah Division of Air Quality's 2017 oil and gas emissions inventory (UDAQ, 2021) but the inventory gives no indication of stack orientation. Regardless, the inventory shows that the majority of these stacks are about 0.6 m in stack height. Based on our measurements, stacks of this height are likely to be horizontal. We recommend that, for modeling applications for the Uinta Basin, any internal combustion engine stack inventoried at less than 1 m height should be assumed to be horizontal, with the characteristics presented in Table 5-1.

Table 5-1. Exhaust stack characteristics of pumpjack engines. Numbers in parenthesis are upper and lower limits of 95% confident intervals from bootstrap sampling.

	Horizontal Stack	Vertical Stack
Number of units	49	9
Stack Height (m)	0.75 (0.8, 0.7)	1.65 (2.2, 1.1)
Stack Diameter (m)	0.1 (0.1, 0.1)	0.1 (0.12, 0.1)
Stack Temperature (°C)	185 (213, 157)	183 (297, 87)
Stack Flow Rate ($m^3\ min^{-1}$)	2.0 (2.5, 1.6)	3.6 (5.6, 2.1)
Stack Exit Velocity ($m\ s^{-1}$)	8.1 (10.9, 6.2)	9.6 (11.6, 7.5)

5.7. Impact of Season on Emissions

We found few meaningful differences across seasons for emissions from a subset of five engines measured in May 2021 and January 2022. Figure 5-15 shows average emissions in both seasons for the five engines. Ambient temperature for the engines in May averaged 20.1°C, compared to 1.8°C in January. Of all the engine parameters measured, the only statistically significant difference between the seasons was emissions of methanol, which were 78 (69, 85)% lower during winter. We don't know why methanol emissions were lower during winter.

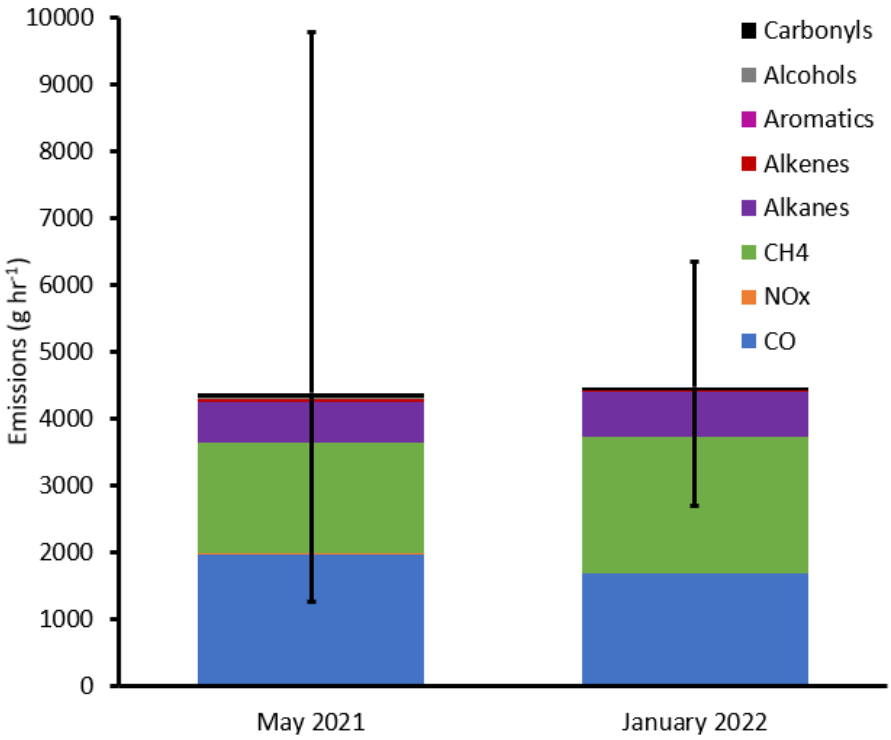

Figure 5-15. Average emissions from five engines measured in May 2021 and January 2022. Whiskers represent 95% confidence intervals for total emissions.

5.8. Comparison Against Inventoried Values

Figure 5-16 and Figure 5-17 are histograms that show the distribution of emissions from our measurements and those of natural gas-fueled pumpjack engines in the latest version of Utah Division of Air Quality's 2017 oil and gas emissions inventory version 1.89, which was released in April 2021 (UDAQ, 2021). Figure 5-16 shows emissions of NO_X and Figure 5-17 shows emissions of volatile organic compounds (VOC). On average, measured NO_X emissions were only 9% of values listed in the inventory (median of 2%), and measured VOC emissions were 15 times higher than values listed in the inventory (median of 10 times). We calculated VOC as all organic compounds other than methane and ethane, following the regulatory definition.

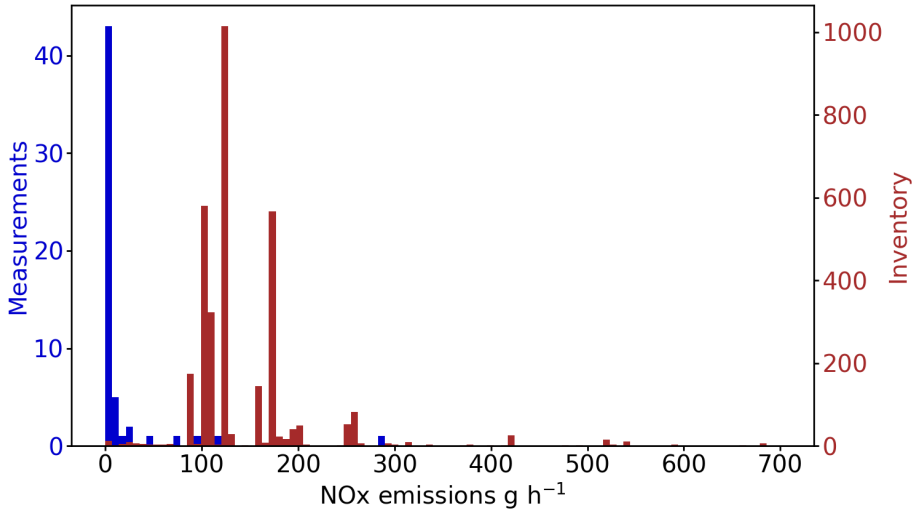

Figure 5-16. Histogram of measured and inventoried NO_X emissions from natural gas-fueled engines. Y-axes show the frequency of occurrence for each emission rate bin.

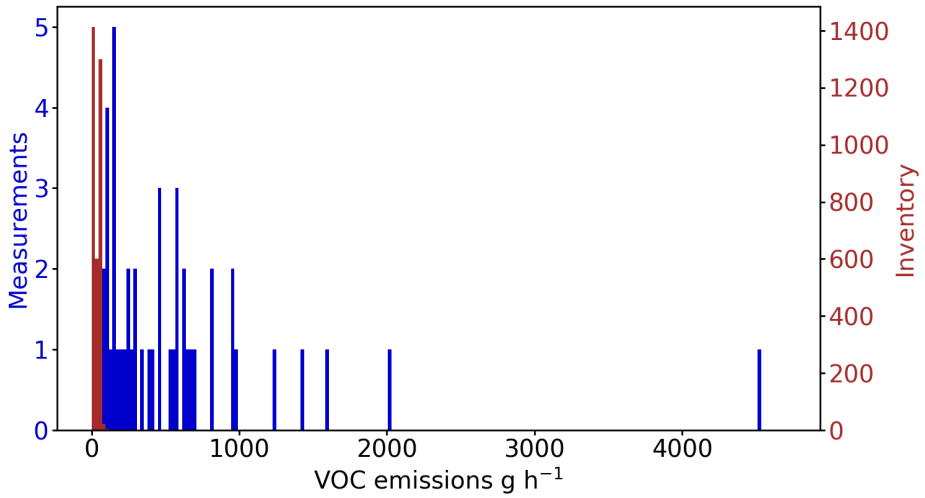

Figure 5-17. Histogram of measured and inventoried volatile organic compound (VOC) emissions from natural gas-fueled engines. The regulatory definition of VOC only includes compounds more reactive than methane and

ethane, and we follow that convention here. Y-axes show the frequency of occurrence for each emission rate bin.

Measured formaldehyde and CO emissions from pumpjack engines were also higher than inventoried values (i.e., formaldehyde emissions listed explicitly in the inventory). Average measured formaldehyde emissions were 6 times the inventory average (Figure 5-18; median measured was 2 times the median inventory), and average measured CO emissions were 9 times the average of all inventory values (Figure 5-19; median measured was 2 times the median inventory).

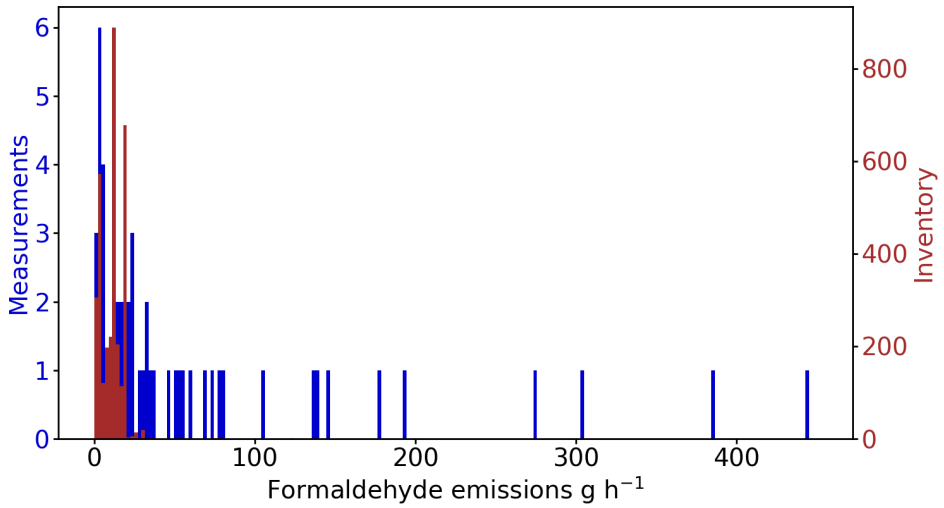

Figure 5-18. Histogram of measured and inventoried formaldehyde emissions from natural gas-fueled engines. Y-axes show the frequency of occurrence for each emission rate bin.

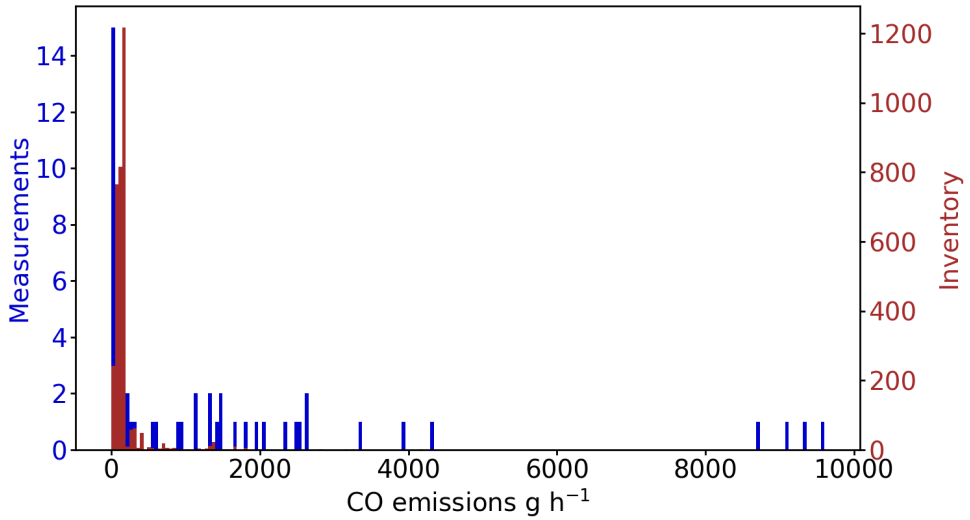

Figure 5-19. Histogram of measured and inventoried CO emissions from natural gas-fueled engines. Y-axes show the frequency of occurrence for each emission rate bin.

Emissions from engines account for 58% of total NO_X and 2% of total VOC emissions in the 2017 inventory. To determine how the results of this study would impact these numbers, we changed emission values for all engines designated as pumping units in the inventory. We did not change emission values for other types of engines. We reduced NO_X emissions from pumping unit engines to 9% of their original values, and we increased VOC emissions to 15 times their original values. After these changes, engines accounted for 37% of NO_X (Figure 5-20) and 15% of VOC emissions (Figure 5-21). These changes reduced total basin-wide emissions of NO_X from oil and gas sources by 33% and increased total VOC emissions by 16%.

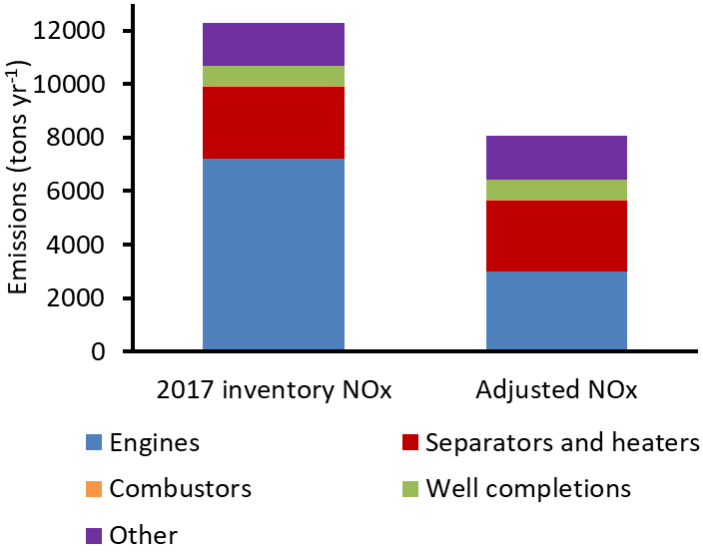

Figure 5-20. Sources of NO_X emissions in the 2017 Utah Division of Air Quality emissions inventory (version 1.89). The left bar shows emissions in the default inventory. The right bar shows emissions adjusted based on the results of this study.

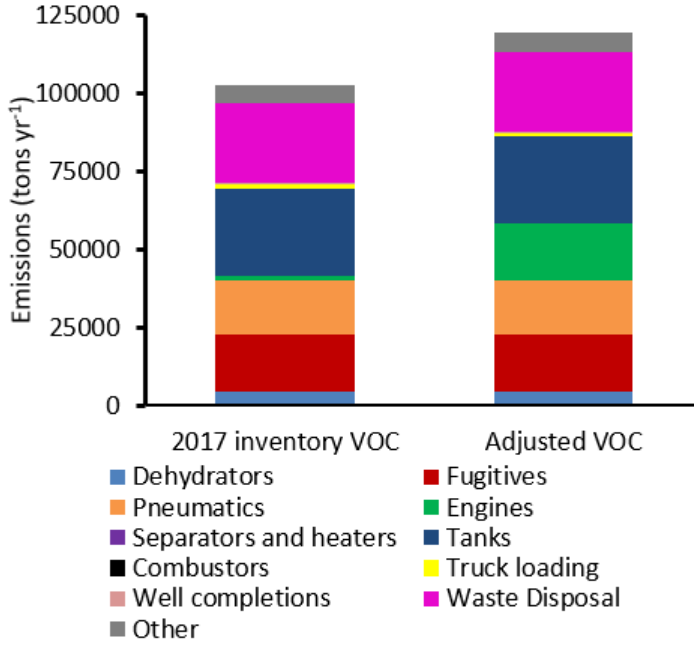

Figure 5-21. Sources of VOC emissions in the 2017 Utah Division of Air Quality emissions inventory (version 1.89). The left bar shows emissions in the default inventory. The right bar shows emissions adjusted based on the results of this study.

6. Implications

This study shows that inventoried emissions from natural gas-fueled engines used to power pumpjacks are too high for NO_X and too low for organic compounds and carbon monoxide. For inventories, engine emissions values typically come from manufacturer specifications or emission factors, such as those provided in EPA's AP-42 emission factor compilation (Alpha-Gamma, 2000; EPA, 1995). The measurements presented here show that engine emissions in real field conditions are different from inventory estimation methods. Accounting for actual engine emissions would change established inventory values substantially.

This study also shows that combustion completeness tends to be low for the two-cycle engines commonly used to power pumpjacks. Many engines we measured had combustion completeness values of less than 50%, meaning that more than 50% of the carbon atoms entering the engine as fuel were exiting the engine uncombusted. The two four-cycle engines we measured had very high combustion completeness, but they had the highest NO_X emissions of all the engines in the study. While it may seem prudent to switch to engines that waste less fuel, obtaining higher combustion completeness comes at the cost of emitting additional NO_X. Our best understanding right now is that reductions in NO_X and organic compound emissions would both result in roughly equivalent reductions in wintertime ozone in the Uinta Basin (Lyman et al., 2021b), but we recommend evaluating how changing engines to increase combustion completeness would impact winter ozone formation before implementing such a strategy. Of course, electric motors emit neither NO_X nor organics, so switching pumping units to electric power would be the best strategy when possible.

This study has resulted in measurements of the magnitude and composition of emissions from natural gas-fueled pumpjack engines that can be implemented in future three-dimensional photochemical modeling efforts.

7. Future Directions

This study showed that emissions from natural gas-fueled pumpjack engines are much different than has been assumed. The magnitude and composition of emissions from other sources in the Uinta Basin may also be different from current assumptions. Some poorly characterized oil and gas-related emission sources include combustors, flares, natural gas-fueled heaters, and glycol dehydrators. Measurements of emissions from these and other sources would provide better data for use in regulatory decision-making and photochemical modeling.

Our team recently conducted preliminary photochemical modeling to determine how the better understanding of pumpjack engine emissions we now have influences photochemical model outputs (Tran et al., 2021). We are now conducting more comprehensive photochemical modeling with these data.

8. Data Management

We will make the final emissions and fuel gas composition dataset available at Utah State University's Digital Commons (https://digitalcommons.usu.edu/), a permanent, indexed archive of research data.

9. Acknowledgments

This work was primarily funded by the Utah Division of Air Quality and the Utah Legislature. Three energy companies allowed our team to access their facilities and provided information used in the study. Chevron provided funding for a liquid chromatograph to analyze samples for carbonyls concentrations in 2020, and we made extensive use of that instrument for the measurements described in this report. An endowment from Anadarko Petroleum Corporation funded the wages of students who participated in the project, including Makenzie Holmes, who processed and analyzed most of the whole-air canister samples.

10. References

Alpha-Gamma, 2000. Emission Factor Documentation for AP-42 Section 3.2, Natural Gas-fired Reciprocating Engines. Alpha-Gamma Technologies, Inc., Raleigh, North Carolina, https://www.epa.gov/sites/default/files/2020-10/documents/b03s02.pdf.

Anneken, D., Striebich, R., DeWitt, M.J., Klingshirn, C., Corporan, E., 2015. Development of methodologies for identification and quantification of hazardous air pollutants from turbine engine emissions. J. Air Waste Manage. Assoc. 65, 336-346.

Brettschneider, J., 1979. Calculation of the air ratio lambda of air-fuel mixtures and the effect of errors in measurement on lambda. Bosch Tech. Ber.;(Germany, Federal Republic of) 6.

CFR, 2021. Code of Federal Regulations Title 40, Part 60, https://www.ecfr.gov/current/title-40/chapter-I/subchapter-C/part-60/.

DEQ, W., 2006. State of Wyoming Air Quality Division Portable Analyzer Monitoring Protocol. Wyoming Department of Environmental Quality, Cheyenne, Wyoming, https://deq.wyoming.gov/aqd/compliance/inspections/.

Edwards, P.M., Brown, S.S., Roberts, J.M., Ahmadov, R., Banta, R.M., deGouw, J.A., Dube, W.P., Field, R.A., Flynn, J.H., Gilman, J.B., Graus, M., Helmig, D., Koss, A., Langford, A.O., Lefer, B.L., Lerner, B.M., Li, R., Li, S.-M., McKeen, S.A., Murphy, S.M., Parrish, D.D., Senff, C.J., Soltis, J., Stutz, J., Sweeney, C., Thompson, C.R., Trainer, M.K., Tsai, C., Veres, P.R., Washenfelder, R.A., Warneke, C., Wild, R.J., Young, C.J., Yuan, B., Zamora, R., 2014. High winter ozone pollution from carbonyl photolysis in an oil and gas basin. Nature 514, 351-354.

EPA, U., 1995. AP 42, Compilation of air pollutant emission factors. Stationary point and area sources 1.

EPA, U., 1999. Compendium Method TO-11A. U.S. Environmental Protection Agency, Research Triangle Park, North Carolina, https://www3.epa.gov/ttnamti1/files/ambient/airtox/to-11ar.pdf.

EPA, U.S., 2020. Addendum SPECIATE Version 5.1 Database Development Documentation. U.S. Environmental Protection Agency, Research Triangle Park, North Carolina, https://www.epa.gov/sites/production/files/2020-07/documents/speciate_5.1.pdf.

Kuppa, K., Nguyen, H., Goldmann, A., Korb, B., Wachtmeister, G., Dinkelacker, F., 2019. Numerical modelling of unburned hydrocarbon emissions in gas engines with varied fuels. Fuel 254, 115532.

Lyman, S., Tran, T., 2015. Measurement of Carbonyl Emissions from Oil and Gas Sources in the Uintah Basin. Utah State University, Vernal, Utah, http://binghamresearch.usu.edu/files/CarbonylEmiss_FnlRprt_31jul2015.pdf.

Lyman, S.N., Holmes, M., Tran, H., Tran, T., O'Neil, T., 2021a. High ethylene and propylene in an area dominated by oil production. Atmosphere *12*, 1.

Lyman, S.N., Mansfield, M.L., 2018. Organic compound emissions from a landfarm used for oil and gas solid waste disposal. J. Air Waste Manage. Assoc. 68, 637-642.

Lyman, S.N., Mansfield, M.L., Tran, H., David, L.M., O'Neil, T., Smuin, D., 2021b. 2021 Annual Report: Uinta Basin Air Quality Research. Utah State University, Vernal, Utah, https://www.usu.edu/binghamresearch/files/reports/UBAQR_2021_AnnualReport.pdf.

Lyman, S.N., Mansfield, M.L., Tran, H.N., Evans, J.D., Jones, C., O'Neil, T., Bowers, R., Smith, A., Keslar, C., 2018. Emissions of organic compounds from produced water ponds I: Characteristics and speciation. Sci. Total Environ. 619, 896-905.

Lyman, S.N., Watkins, C., Jones, C.P., Mansfield, M.L., McKinley, M., Kenney, D., Evans, J., 2017. Hydrocarbon and Carbon Dioxide Fluxes from Natural Gas Well Pad Soils and Surrounding Soils in Eastern Utah. Environ. Sci. Technol. 51, 11625-11633.

Mansfield, M.L., Tran, H.N.Q., Lyman, S.N., Smith, A., Bowers, R., Keslar, C., 2018. Emissions of organic compounds from produced water ponds III: mass-transfer coefficients, composition-emission correlations, and contributions to regional emissions. Sci. Total Environ. 627, 860-868.

Nakamura, H., Asano, I., Adachi, M., Senda, J., 2005. Analysis of pulsating flow measurement of engine exhaust by a Pitot tube flowmeter. International Journal of Engine Research 6, 85-93.

Oliver, W.R., Peoples, S.H., 1985. Improvement of the emission inventory for reactive organic gases and oxides of nitrogen in the South Coast Air Basin. Volume 1. Main report. Final report. Systems Applications, Inc., San Rafael, CA (USA), https://ww3.arb.ca.gov/ei/speciate/r21t40/rf25doc/refnum25.htm.

Restek, 2018. Improve Analysis of Aldehydes and Ketones in Air Samples with Faster, More Accurate Methodology. Restek, Bellefonte, Pennsylvania, https://www.restek.com/en/technical-literature-library/articles/improve-analysis-of-aldehydes-and-ketones-in-air-samples-with-faster-more-accurate-methodology/.

Shimadzu, 2011. Nexera Application Data Sheet No.13: Ultrafast Analysis of Aldehydes and Ketones. Shimadzu, Tokyo, Japan, https://www.shimadzu.com/an/literature/hplc/jpl212018.html.

Tran, H., Lyman, S.N., Mansfield, M.L., 2021. Final Report: Improving volatile organic compound emission estimates for the Uintah Basin. Utah State University, Vernal, Utah, https://www.usu.edu/binghamresearch/files/reports/PodsHC_Final_Report_v1.pdf.

Tran, H.N.Q., Lyman, S.N., Mansfield, M.L., O'Neil, T., Bowers, R.L., Smith, A.P., Keslar, C., 2017. Emissions of organic compounds from produced water ponds II: evaluation of flux-chamber measurements with inverse-modeling techniques. J. Air Waste Manage. Assoc. 68, 713-724.

Tran, T., Tran, H., 2021. Uinta Basin Ozone State Implementation Plan Meteorological Modeling: Weather Research And Forecasting (WRF) Model Performance Evaluation. Utah State Univesrity, Vernal,

Utah, https://www.usu.edu/binghamresearch/files/reports/WRF_UintaBasin_OSIP_MPE_Report_v2.pdf.

Uchiyama, S., Naito, S., Matsumoto, M., Inaba, Y., Kunugita, N., 2009. Improved measurement of ozone and carbonyls using a dual-bed sampling cartridge containing trans-1, 2-bis (2-pyridyl) ethylene and 2, 4-dinitrophenylhydrazine-impregnated silica. Anal. Chem. 81, 6552-6557.

UDAQ, 2021. Statewide Oil and Gas Emissions Inventory, https://deq.utah.gov/air-quality/statewide-oil-gas-emissions-inventory.

Wang, L., Chen, Z., Zhang, T., Zeng, K., 2019. Effect of excess air/fuel ratio and methanol addition on the performance, emissions, and combustion characteristics of a natural gas/methanol dual-fuel engine. Fuel 255, 115799.

Wilson, L., Tran, T., Lyman, S., Pearson, M., McGrath, T., Cubrich, B., 2020. Uinta Basin Composition Study. Utah Department of Environmental quality, Salt Lake City, Utah, https://documents.deq.utah.gov/air-quality/planning/technical-analysis/DAQ-2020-004826.pdf.